Advances in Reliability, Safety and Security, Part 1 – Kołowrocki, Dąbrowska (eds.)
 ISBN 978-83-68136-13-5 (printed), ISBN 978-83-68136-00-5 (electronic)

Advances in Reliability, Safety and Security

ESREL 2024
Monograph Book Series

Improving Spatial Monitoring Of Rain Gauges For Flood Assessment

Chengjun Cao[a], Franck Schoefs[b]

[a] *Nantes Université, École Centrale Nantes, CNRS, GeM, UMR 6183, F-44000 Nantes, France*
[b] *Nantes Université, École Centrale Nantes, CNRS, GeM, UMR 6183, IUML, FR 3473, F-44000 Nantes, France*

Abstract

The flood assessment relies on the reliability of rainfall data. One of the main sources of rainfall data is the rain gauge network. Therefore, an assessment of the current performance of rain gauge stations can be useful in making recommendations for improving the accuracy of rainfall monitoring. In this paper, a spatial rainfall interpolation model for different cases was obtained by adding new virtual rain gauges to an existing rain gauge network. Then the assessment of model uncertainty was completed by cross validation as well as Receiver Operating Characteristic (ROC) curves. Finally, the most recommended locations for adding new rain gauges are obtained by analyzing the uncertainty.

Keywords: rain gauges network distribution, thiessen polygon, uncertainty, roc curve

1. Introduction

Floods are the climate change phenomenon that affects most people in the Atlantic area, causing run-off in urban areas and overflowing rivers through increasingly intense rainfall. In the last 20 years, more than 1,500 lives and 52,000,000 euros have been lost in the EU.

To monitor floods, a crucial component is the monitoring of precipitation in the corresponding area. In actual practice, rain gauges have always been the main source of rainfall data. In countries with higher development and advanced technology, satellites and radars are also playing an increasingly important role in obtaining rainfall data, especially in providing real-time data.

Cross-validation is one of the most commonly used resampling methods and an important tool in many practical applications of statistical learning processes. It can be used to estimate the test errors associated with a given statistical learning method in order to evaluate its performance or to select the appropriate level of flexibility. (Xu et al., 2018) compute the uncertainty of a new rain gauge network by the cross-validation method. This is also the principal method used nowadays to quantify the uncertainty of the network of rain gauge stations. (Marco et al., 2022) use cross-validation to test machine learning-based models used to predict flood risk.

The ROC curve is an analytical tool for selecting the best detection signal. It can give neutral and objective recommendations. The ROC curve is particularly valuable when dealing with binary classification problems, where the performance of a model in distinguishing between two classes needs to be thoroughly examined. (Rouhan and Schoefs, 2003) analyzed and made recommendations for the maintenance of coastal structures using ROC curves in their study.

2. Methodology

The main objective of this study is to improve the spatial reliability of rain gauges network used to measure rainfall data in the study area and to optimize the distribution of the gauges by analyzing specific storm events in a given region. This is followed by an analysis of the model's uncertainty.

The study area chosen for this research is the Landro basin in Galicia. The corresponding rainfall data are obtained from rain gauges, satellite and Meteomapas records in the area. The rainfall data from rain gauges and satellites are combined using the Kriging with External Drift (KED) method and spatially interpolated to obtain a continuous surface of estimated rainfall data from discrete rainfall data points. The key idea is to develop a data base model from data easily available and easily to complete (adding rain gauges). Then new virtual rain gauges are then added to the study area by using the Thiessen polygon method and the high-fidelity model of Meteomapas [https://www.meteogalicia.gal/observacion/meteovisor/xeoHoxe.action?data=26%2F10%2F2023&lnMapa=1&request_locale=es]. Finally, the uncertainty of the model based on the new rain gauge network is quantified by cross validation and the performance of the rain gauge stations is judged by ROC curves.

2.1. Add new virtual rain gauges

The Thiessen polygon method is used in adding new virtual rain gauges in this study which proposed by the Dutch climatologist (Thiessen, 1911) for calculating the average rainfall based on the rainfall at discrete weather stations. Figure 1 illustrates the process of creating Thiessen polygon. All neighboring stations are connected in a triangle and the vertical bisectors of the sides of these triangles are made. The perpendicular bisectors around each station then form a polygon. The rainfall intensity in the polygon area is expressed in terms of the rainfall intensity of a unique station contained within the polygon and is referred to as a Thiessen polygon. Each vertex of a Thiessen polygon is the center of the outer circle of each triangle.

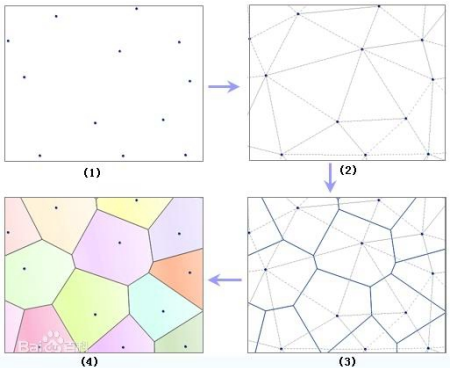

Fig. 1. Thiessen polygon drawing flowchart.

Since the rainfall intensity within the polygon which contains each station can be used to represent the rainfall intensity at the current station. Therefore, each polygon can be considered as the radial area of influence for each station. This allows the weighting of each station within the study area to be obtained. In order to obtain the weight of each rain gauge, by applying the Thiessen polygon, the area that each gauge can influence, i.e., the weight, can be calculated as shown in the (1).

$$p_n = \frac{A_n}{A_s}, \tag{1}$$

where p_n is weight of rain gauge n, A_n is influence area of rain gauge n calculated by Thiessen polygon method, A_s is area of the study region.

2.2. Cross validation for model uncertainty quantification

In the cross-validation process, the data is divided into two parts, i.e., training set and validation set. As shown in Figure 2, the white dots are the validation set and the yellow dots are the test set. In this study, k-fold cross-validation is used. The data is divided into k groups (k = 5 in Figure 2), one of which is set as the validation set and the remaining k-1 groups are the training set.

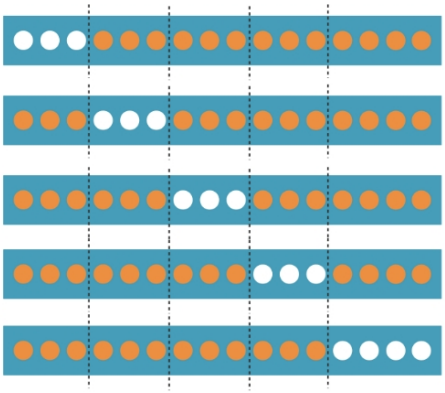

Fig. 2. Cross-validation schematic for 5 groups.

The training set is then used to perform calculations by substituting it into the model to obtain the data corresponding to the validation set. This in turn enables the calculation of the error between the validation set and the results obtained from the model. This loop is repeated, using a different group as the validation set in each loop, until all the data has been validated. Thus, the error situation of the whole set of data in the model is obtained. The error is calculated by (2).

$$E_i(t) = Z_i(t) - G_i(t), \tag{2}$$

E is the error, t is the time step in each event, Z is the results of validation set, and G is the actual rainfall measured by the rain gauge, i the number of the rainfall.

2.3. ROC curve for measuring the impact on decision

The Receiver Operating Characteristic (ROC) Curve is an analytical tool for selecting the best detection signal (Boéro et al., 2009). It can give neutral and objective recommendations. The ROC curve is particularly valuable when dealing with binary classification problems, where the performance of a model in distinguishing between two classes needs to be thoroughly examined. In this study, the ROC curve is used to analyze the performance of the rainfall station in the same way it is used for other NDT performance assessment (Schoefs et al., 2009). The largest the error on a small signal, the worst will be the decision. In order to be able to compare rainstorm events with different intensities, it is first necessary to normalize the error $Z_i - G_i$ and the error combined rainfall Z_n for each event by (3) and (4).

$$(Z_i(t) - G_i(t))_{norm} = \frac{Z_i(t) - G_i(t)}{G_i(t)} \tag{3}$$

$$Z_i(t)_{norm} = \frac{Z_i(t)}{G_i(t)} \tag{4}$$

The ROC curve is a curve based on the Probability of Detection (PoD) and Probability of False Alarm (PFA) (Rouhan and Schoefs, 2003). The PoD is derived from the signal that is synthesized in the sensor as an aggregate value of rainfall and disturbance errors. And the PFA originates from the error. As shown in Figure 3, the plot shows the probability density curves for the error and the combination of error and rainfall with threshold equal to -2 and 0. Then different thresholds are selected and for different thresholds there is a corresponding area under the curve. The value of these areas corresponds to the value of PoD and PFA. Therefore, by selecting different thresholds, a series of PoDs and PFAs can be obtained and the corresponding ROC curves can be obtained. Figure 4 illustrates the ROC curve. And for a particular event, the most desirable state of the model is (PFA, PoD) = (0,1) called NDT-BPP for Best Performance Point (Schoefs et al., 2012). The closer to this point indicates that the model performs better. Meanwhile, when PFA = PoD, it indicates that the results of the model present a bad performance state.

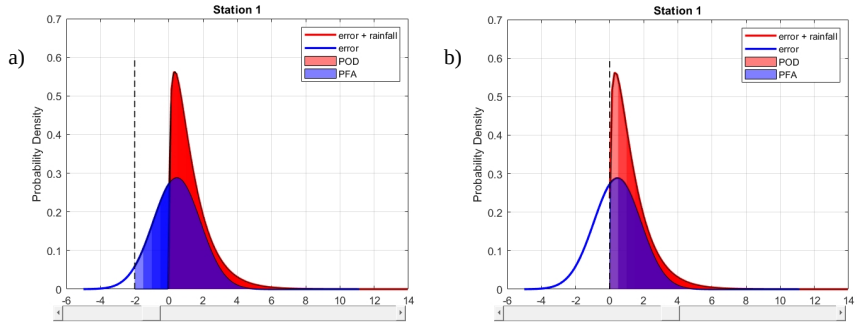

Fig. 3. Probability density curves of signal and error. (a) threshold = -2; (b) threshold = 0.

2.4. Metrics for improving the network

Figure 4 illustrates the ROC curve, where the performance of the model can be judged by the minimal distance d of the curve from (0, 1) (Schoefs and Clément, 2004). A smaller value of d indicates a more efficient model at a selected threshold. Therefore, by calculating d in the model corresponding to all rain gauges in each event, the efficiency of each rain gauge can be clearly obtained, and thus monitoring can be strengthened at weak points.

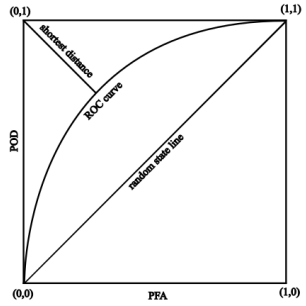

Fig. 4. Schematic of the ROC curve with the minimum distance included.

3. Case study

This study considers the Landro Basin, located in northwestern Spain, which is bordered by the North Atlantic Ocean and through which the Landro River passes. Figure 5 shows a map of the study area which contained the Landro basin and the surrounding area. The area of Landro basin is approximately 199 square kilometers. The Landro River is 42 kilometers long and runs in a north-south direction. The outlet of the Landro River is located at the northern boundary of the basin. Under the influence of the Atlantic Ocean, the region experiences rainy winters with the potential for storms.

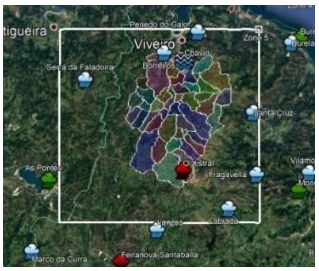

Fig. 5. Map of the Landro basin (with two rain gauges) and the study area containing seven rain gauge stations.

3.1. Data sources

The rain gauge is an instrument used by meteorologists and hydrologists to measure the amount of rainfall that falls over an area during a period of time. The distribution of rain gauges in the Landro Basin is shown in the Figure 5. There are 7 rain gauges in the study area and 2 rain gauge stations located in the Landro basin, with the O Xistra station being established later and recording rainfall data after August 2020. The rain gauge data used in this study is from MeteoGalicia website [https://www.meteogalicia.gal/observacion/estacions/estacions.action?request_locale=gl].

In addition to the rain gauge data, another type of data is available at this location called Meteomapas, which is obtained by spatially modeling the rain gauge data with the radar data. Meteomapas can provide very accurate rainfall close to the real rainfall, so when adding a virtual rain gauge, the Meteomapas data of the corresponding location will be used as the rainfall data of that location.

3.2. Spatial interpolation model used to simulate rainfall

The spatial interpolation method used in this study is KED method. The Kriging method is one of the best linear unbiased estimation methods based on the theory of variance functions and structural analysis. It differs from ordinary estimation methods in that it takes full account of geometric features such as the spatially distributed positions of the information samples and the points to be estimated in relation to each other, as well as structural features such as the spatial correlation between samples. The KED method is different from the traditional kriging method in that it introduces a drift function, which is obtained from the second type of variables (satellite data).

The combination of rain gauge data and satellite data through the KED method can effectively simulate and estimate the rainfall in the study area (Grimes et al., 1999) (Delrieu et al., 2014). Although the accuracy is slightly lower than that of Meteomapas, the cost of the simulation process is lower than it is and it has a wider range of applications.

3.3. Storm events

Generally speaking, a rainfall event with rainfall exceeding 50 millimeters (mm) or more in a 24-hour period is referred to as a storm. For this study, five storm events occurring after August 2020 are selected. In selecting the events, zero or near-zero rainfall across the watershed is used to determine the start and end points of the storms. Table 1 presents information on the storm events.

Table 1. Information of storm events.

Storm index	Start time	End time	Hourly timestep
1	01-Oct-2020 16:00:00	03-Oct-2020 13:00:00	45
2	23-Oct-2020 22:00:00	28-Oct-2020 01:00:00	99
3	01-Oct-2021 22:00:00	03-Oct-2021 16:00:00	42
4	21-Nov-2021 18:00:00	23-Nov-2021 21:00:00	51
5	15-Jan-2023 08:00:00	17-Jan-2023 07:00:00	47

4. Results

The coverage of Meteomapas is smaller than the study area, covering only the Landro Basin, but since the rainfall data for the additional rain gauges can only come from Meteomapas. therefore, when adding rain gauges, the range is restricted to the basin. A total of three separate virtual rain gauges are added to the Landro basin area. During the addition process, it is necessary to ensure that each rain gauge within the study area is approximately roughly equally to ensure the same sphere of influence, thus ensuring maximum efficiency.

The distribution of weights in the study area will be affected not only by the addition of new rain gauges, but also by other rain gauges distributed in neighboring areas outside the study area. Therefore, it is necessary to first select the rain gauges within the study area as well as a circle of neighboring areas outside the coverage area. Plotting the Thiessen polygons of these rain gauges and then restricting them to the study area resulted in a weight distribution map containing the weights of the neighboring rain gauges.

The weight distribution map is shown in Figure 6. Figure 6(a) shows the weight distribution without the addition of the virtual rain gauges and Figure 6(b) shows the weight distribution after the addition of the new rain gauges.

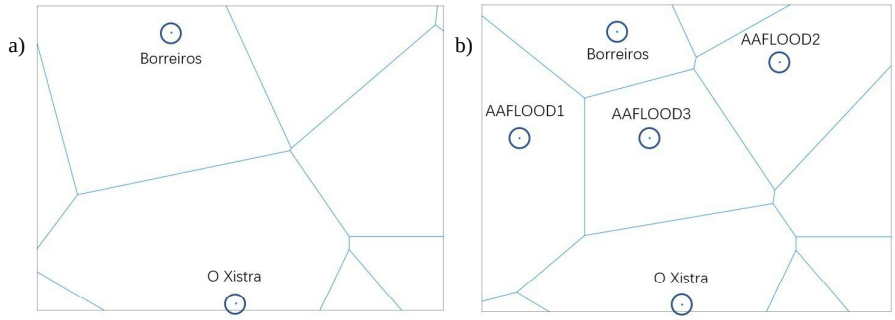

Fig. 6. Map of rain gauge network weight distribution.

Cross-validation is next used to obtain the error of each rain gauge for each time interval of each storm event. Including the additional rain gauges, 10 rain gauge stations are located in the study area. Therefore, in k-fold cross validation, k is taken as 5. This means that the 10 rain gauge stations are categorized into 5 groups, each containing two stations.

After five sets of calculations, the error between the simulated and real values for each station can be obtained. The relationship between rainfall intensity and error can be obtained by matching the error at each time step in each event with the actual rainfall. Taking storm event 1 as an example, the results are shown in Figure 7. From the figure, there is a fairly obvious positive correlation between the rainfall intensity and the error. The higher the rainfall intensity, the higher the error obtained from the simulation.

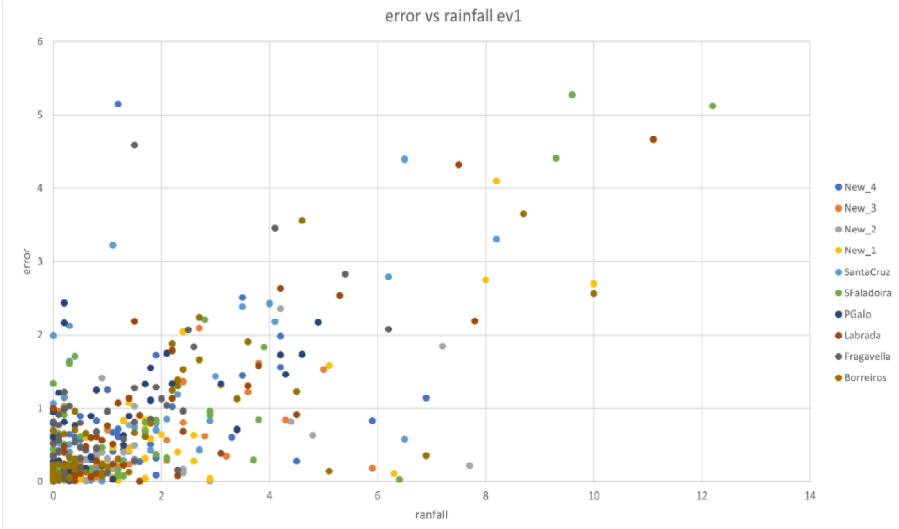

Fig. 7. Relationship between error and rainfall intensity.

In addition, the standard deviations of the errors for different rainfall intensity intervals are analyzed. The results are shown in Figure 8. The figure demonstrates the results and putting the five storm events together, indicates that although it is five different storm events, the standard deviations eventually stabilize and have similar values in all cases. The fact that the values are the same illustrates that the model used in this study is stable across the different scenarios. The deviations of the errors obtained are quite stable. This proves the feasibility and stability of the model.

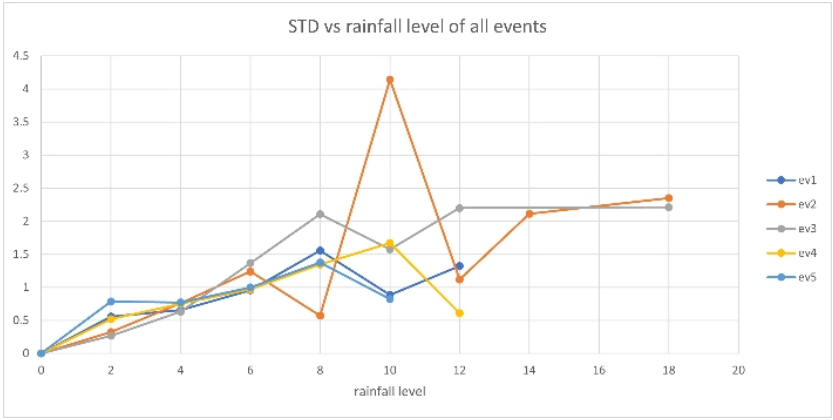

Fig. 8. Standard deviation of the error for different rainfall intensities.

Since the magnitude of the error depends on the storm event and the accuracy of the error is independent of the storm event, the error is normalized. The performance of each rain gauge can be evaluated using the ROC curve.

Since previous steps have found that the distribution of the errors tends to be normal, the normal distribution function will be utilized to calculate the probability density of the errors. That is mainly due to the fact that error is resulting from the sum of independent sources of errors. As for the selection of the signal, the calculated data are all positive and the distribution pattern tends to converge to a gamma distribution, therefore the gamma probability density distribution curve will be used.

Next, the normal distribution curve of the error and the gamma distribution curve of the error integral rainfall are plotted. Figure 9(a) shows this for the 8th rain gauge, AAFLOOD1. Then, the PoD and PFA, plotted against the threshold (-4, 4) with the 0.5 intervals, are plotted for the ROC images of the five storm events containing all stations, as shown in Figure 9(b) to 9(f).

In the ROC plot, there is a line connecting (0, 0) and (1, 1). The points on this line PoD are the same as PFA. Points closer to the upper left corner represent better performance.

The performance of the ROC curve in Storm Time 3 is poor, with much of the data lying below the equal probability line, which means that the probability of false alarms is greater than the probability of detection. In contrast, the ROC curve in Storm Event 5 performs well, with the vast majority of the data located above the equal probability line and stations 3, 7, and 8 very close to the perfect model point. This indicates that the probability of detection is much greater than the probability of false alarm. The performance of the ROC curves for the remaining storm events lies in between and the performance is average.

Preliminary observations indicate better performance at stations 3, 7, and 8, but also vary by storm event and cannot be fully determined. To visualize the performance, the shortest distance from the upper left corner of each curve is extracted. This is shown in Table 2.

Table 2. Shortest distance of each curve.

Station \ Event	1	2	3	4	5	STD	MEAN
1	0.55251	0.69127	0.71153	0.62604	0.37360	0.13652	0.59099
2	0.69391	0.75022	0.70599	0.57043	0.69628	0.06711	0.68337
3	0.53643	0.49745	0.63732	0.35750	0.11047	0.20383	0.42783
4	0.70174	0.65850	0.72438	0.69255	0.53172	0.07647	0.66178
5	0.66704	0.66555	0.60734	0.67008	0.48102	0.08102	0.61821
6	0.67870	0.66523	0.64971	0.62882	0.56294	0.04541	0.63708
7	0.35382	0.51760	0.53219	0.57804	0.11882	0.18853	0.42010
8	0.39685	0.55392	0.70873	0.62027	0.15505	0.21779	0.48696
9	0.59481	0.71709	0.66359	0.48960	0.63918	0.08563	0.62085
10	0.54698	0.53561	0.45039	0.46337	0.57444	0.05436	0.51416

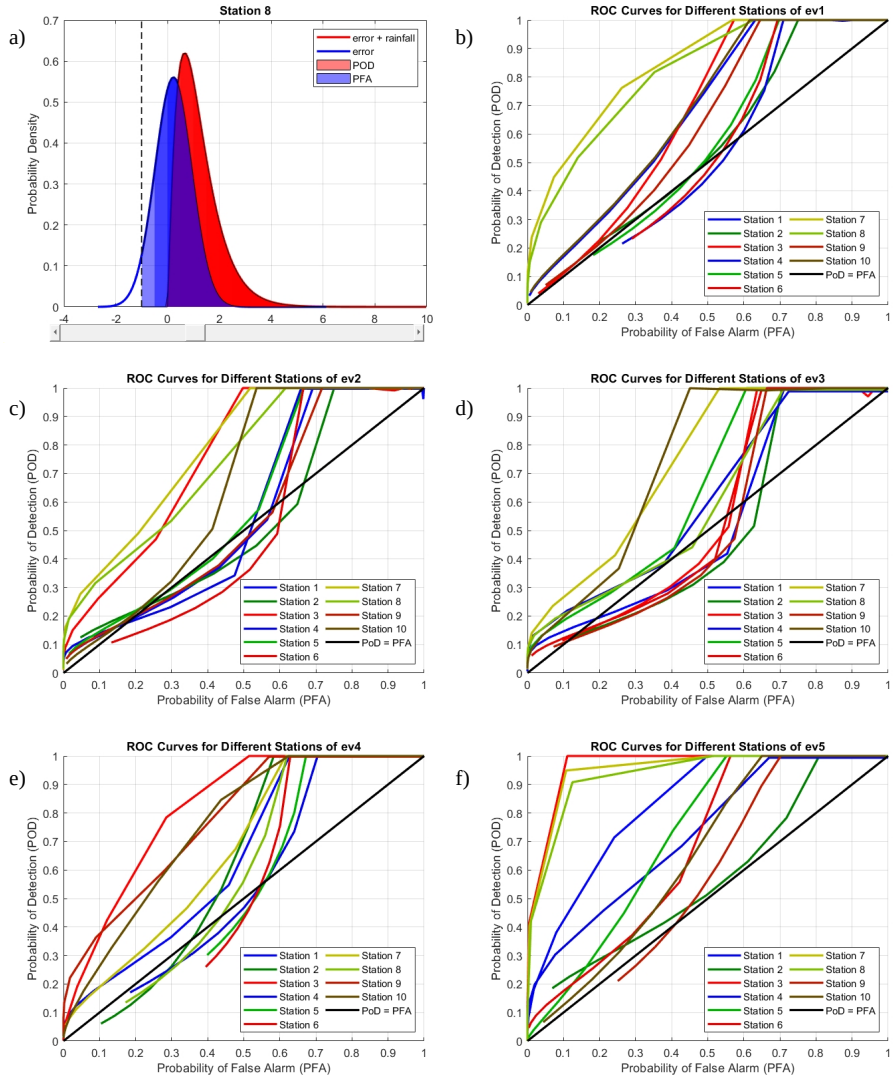

Fig. 9. (a) Probability density distribution; (b)-(f) The ROC curves for all events.

From the Table 2 it is clear that the average of the shortest distances for stations 3, 7 and 8 are indeed smaller than the other sites. However, the well performance is not stable due to the different events. Nevertheless, it can also be observed that station 2 has the longest average distance and, according to the ROC graph, it has a high probability of false alarms, regardless of which event is executed. Therefore, a recommendation can be given accordingly that the highest benefit is obtained if additional surveillance capabilities are added near this station.

5. Conclusion

An inquiry into the amount of rainfall in flood prevention is necessary. Simulated rainfall obtained through spatial interpolation can be proved to be convincing through research and can be spatially interpolated through a combination of rain gauges and satellite data at a lower cost. The weights of each rain gauge should be taken into account in the process of increasing the number of virtual rain gauges in order to maximize the efficiency of the measurements.

The error calculation for interpolating the estimated rainfall was calculated by the cross-validation method, and after comparison, the error and the standard deviation of the error showed a positive correlation with the intensity of rainfall. And since the standard deviation of error shows a stabilizing trend when the rainfall intensity reaches a certain level it shows the reliability of the model. Finally, the rain gauge sites were evaluated by ROC curves and it is highly recommended to strengthen the monitoring at station 2.

Acknowledgements

Thanks to European Committee trough the European Regional Development Found for the support to AAFLOOD Interreg Atlantic Area Project (https://aafloods.eu/).

References

Boero, J., Schoefs, F., Capra, B., 2009. Effect on Risk Based Inspection of spatio-temporal dependence of ROC curves: Study of the corrosion of steel harbour structures.

Delrieu, G., Wijbrans, A., Boudevillain, B., Faure, D., Bonnifait, L., Kirstetter, P.-E., 2014. Geostatistical radar–raingauge merging: A novel method for the quantification of rain estimation accuracy. Adv. Water Resour. 71, 110–124. https://doi.org/10.1016/j.advwatres.2014.06.005

Grimes, D.I.F., Pardo-Igúzquiza, E., Bonifacio, R. 1999. Optimal areal rainfall estimation using raingauges and satellite data. J. Hydrol. 222, 93–108. https://doi.org/10.1016/S0022-1694(99)00092-X

Zanetti, M., Allegri, E., Sperotto, A., Torresan, S., Critto, A., 2022. Spatio-temporal cross-validation to predict pluvial flood events in the Metropolitan City of Venice. J. Hydrol. 612, 128150. https://doi.org/10.1016/j.jhydrol.2022.128150

Rouhan, A., Schoefs, F. 2003. Probabilistic modeling of inspection results for offshore structures. Struct. Saf. 25, 379–399. https://doi.org/10.1016/S0167-4730(03)00016-X

Schoefs, F., Boéro, J., Clément, A., Capra, B. 2012. The αδ method for modelling expert judgement and combination of non-destructive testing tools in risk-based inspection context: application to marine structures. Struct. Infrastruct. Eng. 8, 531–543. https://doi.org/10.1080/15732479.2010.505374

Schoefs, F., Clément, A. 2004. Multiple inspection modelling for decision making and management of jacket offshore platforms: effects of False Alarms, in: First International Forum on Engineering Decision Making, IFED. Stoos, Switzerland.

Schoefs, F., Clément, A., Nouy, A. 2009. Assessment of ROC curves for inspection of random fields. Struct. Saf. 31, 409–419. https://doi.org/10.1016/j.strusafe.2009.01.004

Thiessen, A.H. 1911. Precipitation Averages for Large Areas. Mon. Weather Rev. 39, 1082–1089. https://doi.org/10.1175/1520-0493(1911)39<1082b:PAFLA>2.0.CO;2

Xu, P., Wang, D., Singh, V.P., Wang, Y., Wu, J., Wang, L., Zou, X., Liu, J., Zou, Y., He, R. 2018. A kriging and entropy-based approach to raingauge network design. Environ. Res. 161, 61–75. https://doi.org/10.1016/j.envres.2017.10.038